Chemical Papers (2022) 76:4919–4925
https://doi.org/10.1007/s11696-022-02218-9

ORIGINAL PAPER

Determination of nitrite on manganese dioxide doped reduced graphene oxide modified glassy carbon by differential pulse voltammetry

Betül Yılmaz-Alhan[1] · Gamze Çelik[1] · M. Oguzhan Caglayan[2] · Samet Şahin[2] · Zafer Üstündağ[1]

Received: 10 February 2022 / Accepted: 8 April 2022 / Published online: 25 April 2022

Abstract
A transition metal oxide, MnO_2, doped reduced graphene oxide (rGO) was prepared to develop a 2D-carbon-metal oxide composite modified glassy carbon electrode (GC) for sensitive electrochemical determination of nitrite ion (NO_2^-). GO was first synthesized and reduced to rGO followed by a MnO_2 doping process. The obtained MnO_2-rGO composite was then characterized with Raman spectroscopy, infrared spectroscopy, and scanning electron microscopy techniques. The MnO_2-rGO coated on GC electrodes were electrochemically characterized using cyclic voltammetry, electrochemical impedance spectroscopy and optimized for the determination of NO_2^- using differential pulse voltammetry. A linear calibration curve was obtained between 0.1 and 5.5 µM with LOD and LOQ values of 0.02 µM and 0.06 µM, respectively. The selectivity of the proposed sensor was tested in different substances and no significant interference was found. The sensor validation test showed that the precision (% RSD) and accuracy of the system were around 1.95–2.73% and (−3.5)–2.5%, respectively. Finally, real sample tests with commercially available juice samples and tap water confirmed that the method could detect the spiked NO_2^- in real samples. As a result, the sensitive and easy determination of NO_2^- has been achieved using MnO_2-rGO composite materials in real samples with good recovery values and minimum interference.

Keywords Nitrite analysis · Sensors · MnO_2 doped reduced graphene oxide · Differential pulse voltammetry

Introduction

Nitrite ion (NO_2^-) is a widely used additive in chemical and pharmaceutical industries and can be a serious threat above certain exposure levels in food and water (Iammarino et al. 2013). Although it is mainly utilized for food preservation, it can also be used as a dyeing agent (El-Apasery 2008), corrosion inhibitor (Reou and Ann 2008), and bleach (Ikeda et al. 1999). It is a very well-known pollutant for the environment and human health with fatal ingestion dose levels between 8.7 µM and 28.3 µM (da Silva and Mazo 1998). These values could even go down to 2.17 µM for drinking water (da Silva and Mazo 1998). NO_2^- accumulation in the human body can lead to very serious health problems such as methemoglobinemia due to the irreversible oxidation of hemoglobin. Infant methemoglobinemia which is known as 'the blue baby syndrome' is developed congenital or early in life due to this reaction leading to oxygen deficiency (Chan 2011). Therefore, rapid, sensitive, and easy determination of the dangerous levels of NO_2^- in food samples and drinking water is very important for human health.

The determination of NO_2^- can be problematic due to its easy oxidation but the water solubility facilitates the analysis in aqueous solutions. The current methods in the literature for the determination of NO_2^- include spectroscopic (Yang et al. 2018, Singh et al. 2019), chromatographic (Croitoru 2012, Antczak-Chrobot et al. 2018), and electrochemical methods (Terbouche et al. 2016, Sudarvizhi et al. 2018, Yan et al. 2018). The spectroscopic and chromatographic methods have several limitations such as difficulty in sample preparation, longer test durations, interferences, and selection of column filler (Moorcroft et al. 2001). Electrochemical

✉ Samet Şahin
samet.sahin@bilecik.edu.tr

✉ Zafer Üstündağ
zustundag@gmail.com

[1] Department of Chemistry, Kütahya Dumlupınar University, 43100 Kütahya, Turkey

[2] Department of Bioengineering, Bilecik Şeyh Edebali University, 11230 Bilecik, Turkey

detection, on the other hand, is more advantageous because it can eliminate these problems for the determination of NO_2^-. NO_2^- can be determined using several different approaches such as voltammetric (Esaifan and Hourani 2009, Manea et al. 2010) and amperometric (Baciu et al. 2015). However, the direct NO_2^- determination from aqueous samples are not widely studied especially using electrochemical methods.

Graphene is one of the most widely used one-atom-thick planar sheets comprising a sp^2-bonded carbon structure as two-dimensional materials (Chen et al. 2012). Graphene oxide (GO) and its derivatives such as reduced graphene oxide (rGO) and graphene nanoribbons (GNR) have been more popular than graphene because of their functionality in many applications (Zor et al. 2015, Dideikin and Vul 2019). The derivatives are used as electrode materials and catalysts for electrochemical sensors (You et al. 2015, Çelik et al. 2016). The incorporation of transition metal oxides into 2D-based carbon materials such as MnO_2 and rGO to benefit the enhanced performance of the composite material has been studied in the literature for their good electrocatalytic effect in supercapacitor applications (Jadhav et al. 2019) and the detection of trace metals in water samples (Mnyipika et al. 2021).

Herein, we have developed a detection strategy for the analysis of nitrite in food samples and water using manganese oxide decorated-rGO coated glassy carbon electrodes. (MnO_2-rGO/GC). MnO_2 doped rGO was first prepared and characterized with Raman spectroscopy, infrared spectroscopy (IR) and scanning electron microscopy (SEM) techniques. Then, MnO_2-rGO/GC electrodes were prepared and electrochemically characterized using cyclic voltammetry (CV) and electrochemical impedance spectroscopy (EIS) and optimized for the determination of NO_2^- using differential pulse voltammetry (DPV). The sensitive and easy determination of NO_2^- has been achieved in commercially available juice samples and tap water with good recovery values and minimum interference.

Experimental

Materials

All chemicals used in this study were at analytical grade and purchased from Merck, Fluka, Sigma-Aldrich, and Riedel. Argon (HPLC grade, 99.999%) was used for oxygen removal. Electrochemical experiments were performed at room temperature (24 ± 1 °C) using a three-electrode system where GC electrode (BASi, model: MF-2012), Pt wire and Ag/AgCl (Sat.) electrode as working electrode, auxiliary electrode, and reference electrode, respectively. All aqueous solution and washing steps were performed using ultra-pure water (UPW, 18.2 MΩ cm) which was obtained from Human Power I (Human Corp., Korea).

Preparation of MnO_2 doped reduced graphene oxide electrodes

The schematic for the preparation of the MnO_2 doped reduced graphene oxide electrodes is shown in Fig. 1. Briefly, GO was

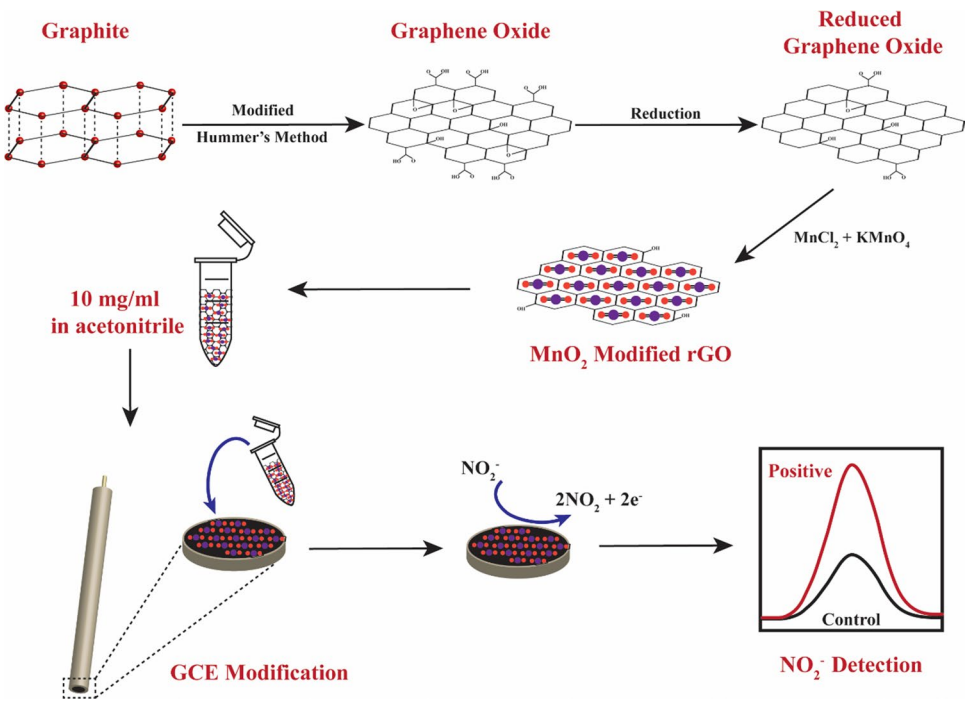

Fig. 1 Schematic representation of the preparation of MnO_2 doped reduced graphene oxide electrodes

synthesized according to modified Hummer's method reported elsewhere (Işık et al. 2021). GO is then reduced using hydrazine (Chua and Pumera 2016). First, 3 g of GO was dispersed in 1 L UPW in an ultrasonic bath (Bandelin, Sonorex, 35 kHz) and mixed with 1 mL of hydrazine under reflux at 80 °C for 12 h. The black suspension was then centrifuged and washed with acetone and UPW multiple times. The final crude product (rGO) was dried in a vacuum oven at 55 °C overnight. To prepare MnO_2 doped rGO electrodes, 26.4 mg rGO and 1.08 g $MnCl_2 + H_2O$ was first mixed in isopropyl alcohol and left in an ultrasonic bath for 1 h. 0.6 g $KMnO_4$ was then dissolved in 20 mL of UPW and added to the previous mixture (Erkal et al. 2015, Güleşen et al. 2019, Erkal-Aytemur et al. 2019). The final mixture is stirred at 85 °C for 30 min and centrifuged for 10 min at 5000 rpm. The solid precipitate was washed with UPW three times and left to dry in a vacuum oven at 55 °C overnight. MnO_2 doped rGO electrodes were finally obtained by drop coating 5, 10, 15, 20 and 25 µL suspensions of 10 mg of MnO_2-rGO in 1 mL acetonitrile on GC electrode surface and denoted as MnO_2-rGO/GC. 15 µL suspensions of GO and rGO in acetonitrile were also coated on GC electrodes for comparison purposes and denoted as GO/GC and rGO/GC, respectively.

Characterization of electrodes and sensor calibration

Before any optimization experiments, GC, GO/GC, rGO/GC, and MnO_2-rGO/GC electrodes were characterized using CV and EIS in the presence of 2 mM $K_3Fe(CN)_6/K_4Fe(CN)_6$ redox couple in 0.1 M KCl. Infrared spectroscopy (Bruker, Tensor-27, Germany), SEM–EDX (Nova, NanoSEM-650, Belgium), and Raman spectroscopy (Horiba, Jobin-Ivon, France) analysis were also used for the characterization of GO, rGO, and MnO_2-rGO. The effect of the coating volume and the calibration of the prepared sensor was performed using the DPV in the presence of 5 µM NO_2^- and (0.1–5.5 µM) NO_2^- concentrations, respectively. The stability of the prepared sensor was calculated using intraday and inter-day (7 consecutive days) experiments. Interference studies were also conducted using 100 µM Na^+, Ca^{2+}, Zn^{2+}, Cu^{2+}, NO_3^-, Cl^-, SO_3^{2-}, SO_4^{2-}; citric acid, ascorbic acid, catechol, and hydroquinone to demonstrate the selectivity of the sensor. Finally, real sample tests were performed using different beverages and tap water. The beverages were first filtered and diluted before electrochemical tests.

Results and discussion

The successful modification of different electrode configurations was first confirmed using CV and EIS using a redox couple as shown in Fig. S1a and 1b. The voltammograms show that MnO_2-rGO/GC electrode had the highest anodic peak current ca. 29.6 ± 0.08 µA. There is a significant current increase response of 80% from rGO/GC indicating the high electrocatalytic performance of the MnO_2-rGO/GC electrode. Furthermore, EIS results (Fig. S1b) show that a low charge transfer resistance (R_{ct}) of the MnO_2-rGO/GC electrode compared to other modified electrodes and the bare electrode was obtained. This is because of the highly conductive nature of the MnO_2-rGO/GC electrode allowing fast electron transfer between the redox couple and the electrode surface. The experimental data were fitted using the Randles equivalent circuit (Garyfallou et al. 2017). The equivalent circuit designs and calculated R_{ct} values of the redox couple on the electrode are given in Table S1. The electrochemical characterization results revealed that CV and EIS results were in parallel with each other confirming the electron transfer rates of the redox couple were increased with MnO_2-rGO/GC electrode.

Figure 2a shows the D and G bands of graphite, GO, rGO, and MnO_2-rGO obtained from Raman spectroscopy. The ID/IG Raman intensity ratios of graphite, GO, rGO, and MnO_2-rGO were 0.06, 0.94, 1.10, 1.02, respectively. This shows that the D band intensity of GO is increased compared to graphite because of the change in sp^2 hybridization due to the chemical oxidation of graphite. The ID/IG Raman intensity ratio of rGO is higher than GO indicating a further change in sp^2 hybridization due to reduction GO. The ratio of MnO_2-rGO was decreased compared to rGO but still was slightly over 1. Furthermore, the characteristic peak of Mn–O lattice vibrations can also be seen at around 625 cm^{-1}. These Raman spectroscopy results are similar to previously reported literature (Han et al. 2014).

IR spectra of GO, rGO, and MnO_2-rGO are also given in Fig. 2b. The IR spectrum of GO shows a broad peak between 3000 and 3700 cm^{-1} corresponding to O–H stretching of –COOH (Yeter et al. 2021). The C=O (carbonyl) and C–O–C peaks appeared at 1700 cm^{-1} and 1280 cm^{-1}, respectively (Erkal-Aytemur et al. 2019). In the IR spectrum of rGO, the intensity of the peaks that appeared in the spectrum of GO is dramatically decreased but C=C stretching was seen at 1550 cm^{-1} (Uluok et al. 2015). The IR spectrum of MnO_2-rGO revealed that the C–N peak also appeared at 1280 cm^{-1} in addition to the peaks that appeared in the spectrum rGO (Çelik et al. 2016).

SEM micrographs of GO, rGO, and MnO_2-rGO show typical structural patterns of corresponding graphene structures (Fig. 2). The two-dimensional sheet-like structure with visible edges of individual sheets is evident of the multiple lamellar layer structure of GO (https://doi.org/10.4236/graphene.2017.61001). On the other hand, rGO micrograph shows a similar structure to its predecessor, but more wrinkled and possibly smaller sheets were obtained after the reduction (https://doi.org/10.3390/nano9081180). The micrograph

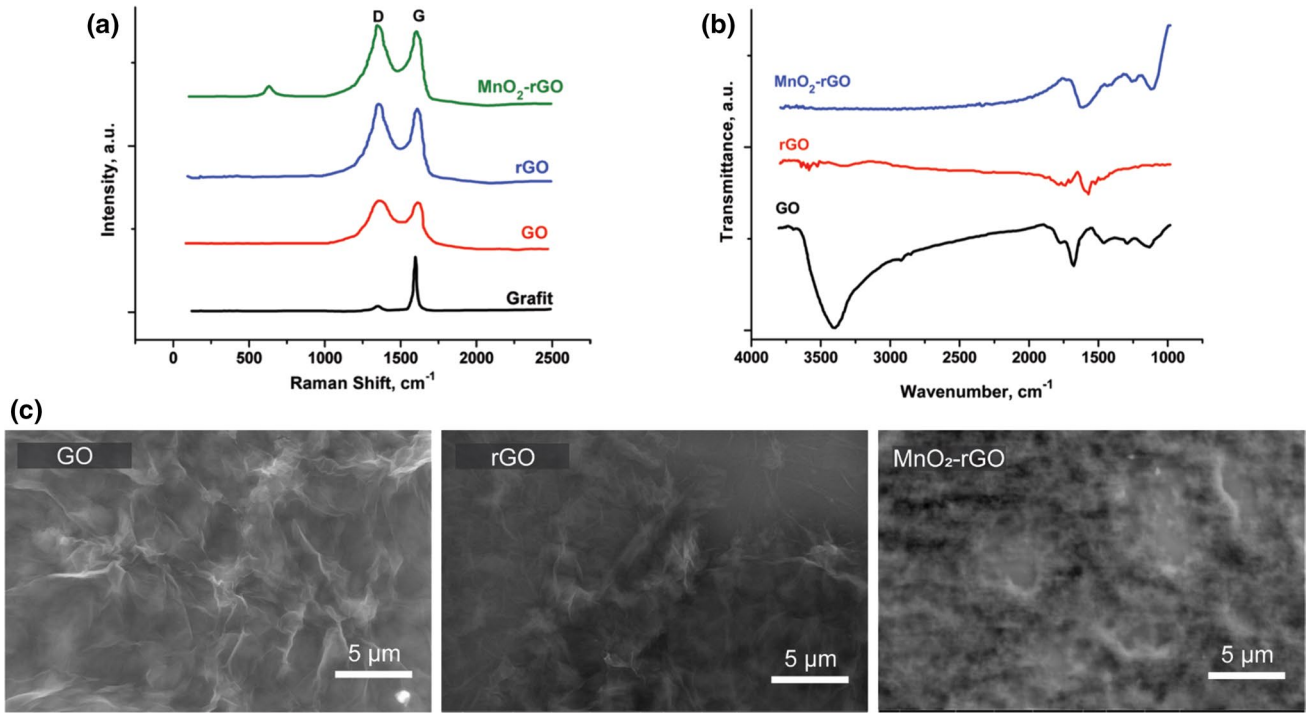

Fig. 2 **a** Raman and **b** IR spectra **c** SEM micrographs of different electrode materials

of MnO2-rGO shows typical but non-uniform clusters of oxide crystals (https://doi.org/10.1007/s00604-018-3064-3). MnO_2 existence on rGO sheets was also confirmed by EDX analysis (Fig S2). The mean percentages of the elements (by weight) were as follows: 68.48% C, 27.41% O, 3.30% Mn, and ~ 0.81% of other impurities.

Although MnO_2-rGO/GC electrode showed better electroanalytical performance than other modified and/or unmodified electrodes in the presence of a redox couple, further voltammetric analysis has been performed to confirm the electrocatalytical effect of different electrode configurations for NO_2^- oxidation. Figure 3a shows the CV results of coated GC electrodes tested in 0.1 mM NO_2^- and the anodic peak potentials are given in Table S2. All modified GC electrodes showed catalytic activity for NO_2^- oxidation in which MnO_2-rGO/GC electrode showed the highest peak current of 48.2 ± 0.8 µA. These results of MnO_2-rGO/GC also confirmed that the electrooxidation of NO_2^- was a diffusion-controlled process (Fig. S3); therefore, the quantitative determination of NO_2^- can be performed using voltammetric techniques.

Upon confirming the suitability of the MnO_2-rGO/GC electrode and the electrochemical technique for quantitative NO_2^- analysis, optimization studies have been conducted. First, the amount of MnO_2-rGO was optimized by coating different volumes of 10 mg/ml MnO_2-rGO (in acetonitrile) suspension on GC electrode and dried under IR lamb. The resulting electrodes were tested using DPV between 0.4 V and 1.2 V (vs Ag/Cl) in the presence of 5 µM NO_2^- (in PBS, pH 7). Figure 3b, c shows that the best peak current was obtained for 15 µL coating (~ 2 mg/cm^2 surface coverage); therefore, it was chosen as an optimized coating volume.

Next, the calibration curve was obtained using DPV for the optimized suspension coating volume for 0.1 µM–5.5 µM NO_2^- concentration range in PBS, pH 7 (Fig. 3d). The anodic peak currents were then plotted against respective concentrations (Fig. 3e) and the analytical performance parameters are calculated as shown in Table 1. The calibration curve was linear between 0.1 µM and 5.5 µM NO_2^- concentration range with a sensitivity value of ca. 5.18 µA/µM. The LOD and LOQ of the proposed analysis method were calculated as 0.02 µM (S/N ratio of 3) and 0.06 µM, respectively. A comparison of the electroanalytical sensors proposed in this study with other reported electrodes is listed in Table 2. The developed sensor performance is comparable with the recently published sensors for NO_2^- determination. The performance of the developed nitrite sensor shows high stability, repeatability, and selectivity.

For the validation of the developed analysis strategy, precision and accuracy tests were also performed using two different NO_2^- concentrations (2 and 4 µM). The inter-day and intra-day experiments were revealed that the RSD % and RE % of the system were around 1.95–2.73% and (− 3.5)–2.5%, respectively. The validation experiments were conducted with 6 individually prepared electrodes, and the results are presented in Table 3. The results

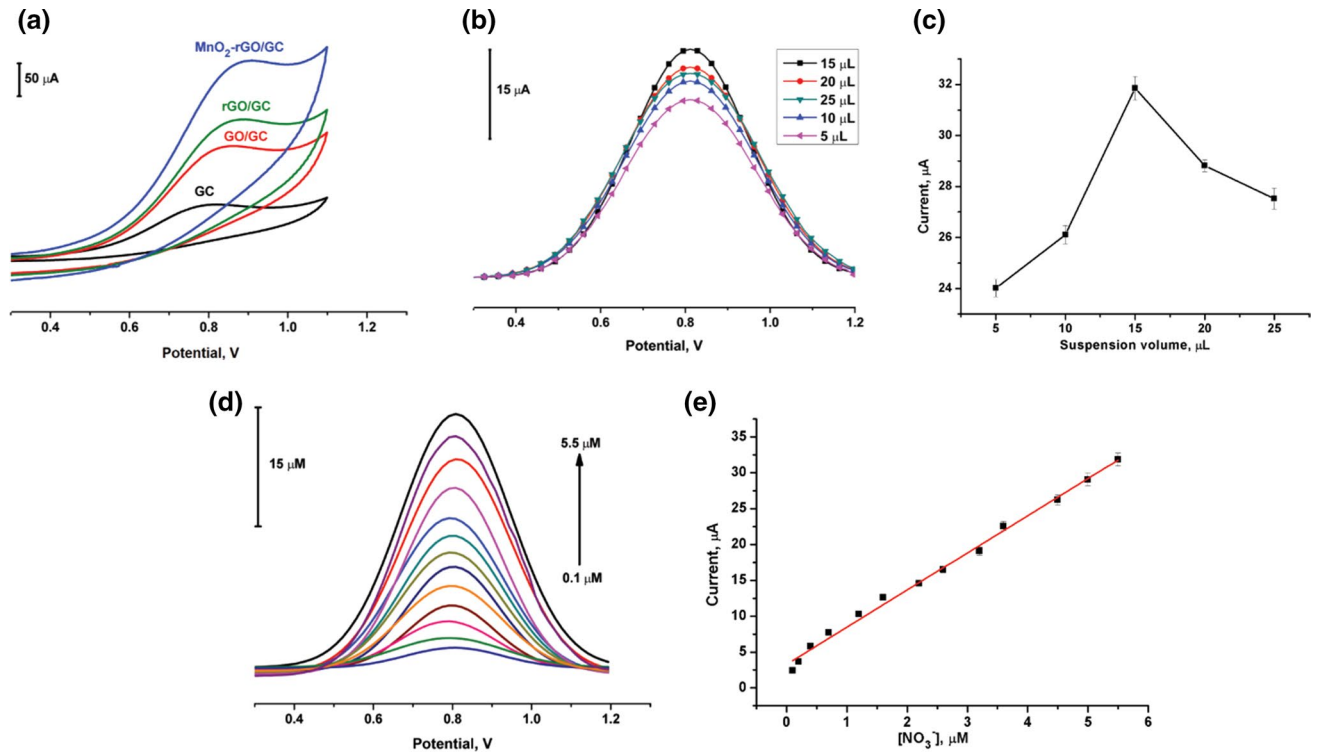

Fig. 3 **a** CVs of different electrode configurations tested in PBS containing 0.1 mM NO2⁻. (in PBS, pH 7). **b** DPVs of MnO2-rGO/GC electrode coated with different volumes of MnO2-rGO. **c** Peak currents obtained from DPVs performed. **d** DPVs of MnO2-rGO/GC electrode using optimized parameters in the presence of 5 µM NO2⁻ (in PBS, pH 7). **e** Calibration curve obtained from d using peak current values for each NO2⁻ concentration.

Table 1 Analytical performance parameters of the developed method

Analytical parameters	Results
Linear concentration range, µM	0.1–5.5
Fitted equation, *Ip* (µA) and NO_2^- (µM)	$Ip = 5.1757[NO_2^-] + 3.3014$
Standard error of the slope	0.1150
Standard error of the intercept	0.3419
R^2	0.9941
LOD, µM (*S*/*N* = 3)	0.02
LOQ, µM	0.06

indicate that the method is working within a negligible margin of error in terms of its precision and accuracy for both inter and intra-day conditions.

Several different potential interfering anion and molecules were also investigated to test the sensitivity of the developed method. 100 µM of each interfering substance was tested with 10 µM NO_2^- and the obtained results are presented in Table 4. The results showed that the change in the peak current was not significant; therefore, the method was considered as sensitive to NO_2^- in the presence of the selected interferences.

The real sample tests were performed using commercially available juices and water. Different juices were first filtered and diluted for the recovery experiments. Table 5 shows the obtained results for three different juices and tap water for six individually prepared electrodes per sample. The results showed that the method could detect the spiked NO_2^- within a confidence level of 95%.

Conclusion

A sensitive and rapid electrochemical NO_2^- sensor has been developed using MnO_2 doped rGO coated on GC electrodes. Spectroscopic and microscopic characterization techniques confirmed the MnO_2 existence on rGO sheets and electrochemical characterization showed electroanalytical activity of MnO_2. Furthermore, MnO_2-rGO/GC electrodes showed electrocatalytic activity toward NO_2^- oxidation in aqueous media. DPV was utilized to obtain the linear calibration curve which has LOD and LOQ values of 0.02 µM and 0.06 µM, respectively. The linear detection range was found between 0.1 µM and 5.5 µM, and the sensor showed very good selectivity in the presence of thirteen different interfering substances.

Table 2 A short review of the electroanalytical performance parameters published in the literature using different electrochemical methods for NO_2^- determination

Electrode	Method	Linear range (μM)	LOD (μM)	References
CoTM-QOPc/GCE	CV	0.3–120	0.1	(Jilani et al. 2020)
f-ZnO@rFGO/GCE	LSV	100–3000	33.0	(Marlinda et al. 2015)
rGO/ZnO/GCE	CA	20–520	1.36	(Rashed et al. 2020)
CdTe/QD-CTAB/Chit-MWCNT/GCE	SWV	1–600	0.30	(Hu et al. 2017)
Graphene/HA/GCE	SWV	3–950	0.025	Lavanya et al. 2015
Fe_2O_3-rGO/GCE	DPV	0.05–780	0.015	(Radhakrishnan et al. 2014)
rGO/$MnFe_2O_4$/PANI/GCE	DPV	0.05–12	0.045	(Sahoo vd. 2020)
oxMoS_2-NSs/GCE	CA	1 – 386	0.028	(Zou et al. 2021)
poly 1,8-DAN /Cys/CB/GCE	DPV	20–210	0.25	(Salhi et al. 2022)
Si/C/Al/$SiPy^+Cl^-$/GCE	CA	0.2–280	0.01	(Alsaiari et al. 2022)
Au@CQDs-MXene/GCE	DPV	1–3200	0.078	(Feng et al. 2022)
Fe-BZIM-Nafion/SCE	CP	1–100	0.53	(Ficca et al. 2022)
Mn-rGO-GCE	DPV	0.1–5.5	0.02	This work

Table 3 Precision and accuracy results for inter and intra-day conditions

		Added sample (NO_2^-)	
		2 μM	4 μM
Inter-day	Found	1.93 ± 0.05	4.03 ± 0.11
	RSD %	2.59	2.73
	RE %	− 3.50	0.75
Intra-day*	Found	2.05 ± 0.04	4.09 ± 0.08
	RSD %	1.95	1.96
	RE %	2.50	2.25

Error bars are sample standard deviations $N = 6$ samples

*Seven consecutive days

Table 4 The effect of interfering substances on peak current change in the presence of 10 μM NO_2^- in 0.1 M PBS (pH = 7.0)

Interfering substance	Concentration (mol/L)	Peak current change (%)
Na^+	1.0×10^{-2}	1.83
Ca^{2+}	1.0×10^{-2}	− 1.17
Zn^{2+}	1.0×10^{-2}	2.35
Cu^{2+}	1.0×10^{-2}	3.06
NO_3^-	1.0×10^{-2}	− 2.84
Cl^-	1.0×10^{-2}	− 0.96
SO_3^{2-}	2.0×10^{-3}	− 1.24
I^-	5.0×10^{-4}	2.24
Citric acid	1.0×10^{-2}	0.88
Ascorbic acid	1.0×10^{-3}	2.41
Catechol	1.0×10^{-4}	− 4.08
Hydroquinone	1.0×10^{-4}	3.31
Dopamine	1.0×10^{-5}	− 2.27

Table 5 The recovery values of NO_2^- from real samples.

Real sample	Added (μM)	Found (μM)	Recovery (%)
Apricot juice	5.0	4.98	99.6
Orange juice	5.0	5.08	101.6
Peach juice	5.0	5.05	101.0
Tap water	5.0	5.16	103.2

$N = 6$ samples

The validation of the sensor was further confirmed with inter and intra-day experiments resulting in RSD % and RE % values around 1.95–2.73% and (− 3.5)–2.5%, respectively. These precision and accuracy values suggest that the proposed sensor may be very advantageous for the use of the sensor during same-day or consecutive days for food/water quality testing on site. The detection of the spiked NO_2^- in real samples showed that the sensitive and easy determination of NO_2^- could be achieved using MnO_2-rGO composite materials with good recovery values and minimum interference. The proposed sensor may be useful for food safety and water-quality monitoring based on its comparable performance with the most recent studies in the literature.

Supplementary Information The online version contains supplementary material available at https://doi.org/10.1007/s11696-022-02218-9.

Declarations

Conflict of interest The authors declare that they have no known competing financial interests or personal relationships that could have appeared to influence the work reported in this paper.

References

Alsaiari M et al (2022) SiO2/Al2O3/C grafted 3-n propylpyridinium silsesquioxane chloride-based non-enzymatic electrochemical sensor for determination of carcinogenic nitrite in food products. Food Chem 369:130970

Antczak-Chrobot A et al (2018) The use of ionic chromatography in determining the contamination of sugar by-products by nitrite and nitrate. Food Chem 240:648–654

Baciu A et al (2015) Simultaneous voltammetric/amperometric determination of sulfide and nitrite in water at BDD electrode. Sensors 15(6):14526–14538

Çelik GK et al (2016) 3, 8-Diaminobenzo [c] cinnoline derivatived graphene oxide modified graphene oxide sensor for the voltammetric determination of Cd 2+ and Pb 2+. Electrocatalysis 7(3):207–214

Chan TY (2011) Vegetable-borne nitrate and nitrite and the risk of methaemoglobinaemia. Toxicol Lett 200(1–2):107–108

Chen D et al (2012) Graphene oxide: preparation, functionalization, and electrochemical applications. Chem Rev 112(11):6027–6053

Chua CK, Pumera M (2016) The reduction of graphene oxide with hydrazine: elucidating its reductive capability based on a reaction-model approach. Chem Commun 52(1):72–75

Croitoru MD (2012) Nitrite and nitrate can be accurately measured in samples of vegetal and animal origin using an HPLC-UV/VIS technique. J Chromatogr B 911:154–161

da Silva SM, Mazo LH (1998) Differential pulse voltammetric determination of nitrite with gold ultramicroelectrode. Electroanalysis 10(17):1200–1203

Dideikin AT, Vul AY (2019) Graphene oxide and derivatives: the place in graphene family. Front Phys 6:149

El-Apasery MA (2008) Solvent-free one-pot synthesis of some azo disperse dyes under microwave irradiation: dyeing of polyester fabrics. J Appl Polym Sci 109(2):695–699

Erkal A et al (2015) An electrochemical application of MnO2 decorated graphene supported glassy carbon ultrasensitive electrode: Pb2+ and Cd2+ analysis of seawater samples. J Electrochem Soc 162(4):H213

Erkal-Aytemur A et al (2019) Electrocatalytic effect of nano-wrinkled layer carbonaceous electrode: determination of folic acid by differential pulse voltammetry. Chem Pap 73(6):1369–1376

Esaifan M, Hourani MK (2009) Indirect voltammetric method for determination of nitrogen dioxide in the ambient atmosphere. Jordan J Chem 4(4):367–375

Feng X et al (2022) Au@ carbon quantum Dots-MXene nanocomposite as an electrochemical sensor for sensitive detection of nitrite. J Colloid Sci 607:1313–1322

Ficca VC et al (2022) Sensing nitrite by iron-nitrogen-carbon oxygen reduction electrocatalyst. Electrochim Acta 402:139514

Garyfallou G-Z et al (2017) Electrochemical detection of plasma immunoglobulin as a biomarker for alzheimer's disease. Sensors 17(11):2464

Güleşen M et al (2019) Evaluation of nanomanganese decorated typha tassel carbonaceous electrode: preparation, characterization, and simultaneous determination of Cd2+ and Pb2+. Chem Pap 73(11):2869–2878

Han G et al (2014) Sandwich-structured MnO 2/polypyrrole/reduced graphene oxide hybrid composites for high-performance supercapacitors. RSC Adv 4(20):9898–9904

Iammarino M et al (2013) Endogenous levels of nitrites and nitrates in wide consumption foodstuffs: results of 5 years of official controls and monitoring. Food Chem 140(4):763–771

Ikeda T et al (1999) Sulfuric acid bleaching of kraft pulp II: behavior of lignin and carbohydrate during sulfuric acid bleaching. J Wood Sci 45(4):313–318

Işık D et al (2021) Electrochemical impedimetric detection of kanamycin using molecular imprinting for food safety. Microchem J 160:105713

Jadhav S et al (2019) Manganese dioxide/reduced graphene oxide composite an electrode material for high-performance solid state supercapacitor. Electrochim Acta 299:34–44

Manea F et al (2010) Simultaneous electrochemical determination of nitrate and nitrite in aqueous solution using Ag-doped zeolite-expanded graphite-epoxy electrode. Talanta 83(1):66–71

Mnyipika SH et al (2021) MnO2@ reduced graphene oxide nanocomposite-based electrochemical sensor for the simultaneous determination of trace Cd (II), Zn (II) and Cu (II) in water samples. Membranes 11(7):517

Moorcroft MJ et al (2001) Detection and determination of nitrate and nitrite: a review. Talanta 54(5):785–803

Reou J, Ann K (2008) The electrochemical assessment of corrosion inhibition effect of calcium nitrite in blended concretes. Mater Chem Phys 109(2–3):526–533

Salhi O et al (2022) Cysteine combined with carbon black as support for electrodeposition of poly (1, 8-Diaminonaphthalene): application as sensing material for efficient determination of nitrite ions. Arab J Chem 15:103820

Singh P et al (2019) A review on spectroscopic methods for determination of nitrite and nitrate in environmental samples. Talanta 191:364–381

Sudarvizhi A et al (2018) Amperometry detection of nitrite in food samples using tetrasulfonated copper phthalocyanine modified glassy carbon electrode. Sens Actuators B Chem 272:151–159

Terbouche A et al (2016) A new electrochemical sensor based on carbon paste electrode/Ru (III) complex for determination of nitrite: electrochemical impedance and cyclic voltammetry measurements. Measurement 92:524–533

Uluok S et al (2015) Nanocharacterization of the graphene oxide terminated platform on polycrystalline gold surface. J Comput Theor Nanosci 12(8):1787–1794

Yan M et al (2018) Research progress on nitrite electrochemical sensor. Chin J Anal Chem 46(2):147–155

Yang H et al (2018) Diazo-reaction-based SERS substrates for detection of nitrite in saliva. Sens Actuators B Chem 271:118–121

Yeter EÇ et al (2021) An electrochemical label-free DNA impedimetric sensor with AuNP-modified glass fiber/carbonaceous electrode for the detection of HIV-1 DNA. Chem Pap 75(1):77–87

You J-M et al (2015) New approach of nitrogen and sulfur-doped graphene synthesis using dipyrrolemethane and their electrocatalytic activity for oxygen reduction in alkaline media. J Power Sour 275:73–79

Zor E et al (2015) An electrochemical and computational study for discrimination of d-and l-cystine by reduced graphene oxide/β-cyclodextrin. Analyst 140(1):313–321

Zou HL et al (2021) High-valence Mo (VI) derived from in-situ oxidized MoS2 nanosheets enables enhanced electrochemical responses for nitrite measurements. Sens Actuators B Chem 337:129812